Effects of zinc nitrate and HMTA on the formation mechanisms of ZnO nanowires on Au seed layers

Clément Lausecker, Bassem Salem, Xavier Baillin, Vincent Consonni

To cite this version:

Clément Lausecker, Bassem Salem, Xavier Baillin, Vincent Consonni. Effects of zinc nitrate and HMTA on the formation mechanisms of ZnO nanowires on Au seed layers. Crystal Growth & Design, 2023, 23 (4), pp.2941-2950. 10.1021/acs.cgd.3c00068 . hal-04060117

HAL Id: hal-04060117
https://hal.science/hal-04060117v1

Submitted on 6 Apr 2023

Effects of Zinc Nitrate and HMTA on the Formation Mechanisms of ZnO Nanowires on Au Seed Layers

Clément Lausecker,[1,2,3] Bassem Salem,[2] Xavier Baillin,[3] and Vincent Consonni.[1*]*

[1] Université Grenoble Alpes, CNRS, Grenoble INP, LMGP, F-38000 Grenoble, France

[2] Université Grenoble Alpes, CNRS, CEA/LETI-Minatec, Grenoble INP, LTM, F-38054 Grenoble, France

[3] Université Grenoble Alpes, CEA, LETI, F-38000 Grenoble, France

Correspoding authors: bassem.salem@cea.fr and vincent.consonni@grenoble-inp.fr

ABSTRACT

The ability to form ZnO nanowire arrays with dedicated morphological properties is crucial for the development of efficient piezoelectric devices such as piezoelectric nanogenerators and sensors. However, their integration typically requires the use of metallic seed layers for their synthesis by chemical bath deposition, from which their morphological control is still very limited. In this context, the formation mechanisms of ZnO nanowires from Au seed layers are carefully investigated for different precursor (*i.e.* zinc nitrate and hexamethylenetetramine) concentrations in the range of 1 to 100 mM, where drastic variations of the morphological properties are observed. By coupling *in situ* pH measurements and thermodynamic computations, we perform an in-depth analysis of the thermodynamic properties of the chemical bath, where the predominent role of the NO_3^- ions in the evolution of the pH of the chemical bath is revealed. An original approach is further developed to carefully determine the hydrolysis ratio of HMTA molecules, which is found to vary in the range of 20 – 45 % with the precursor concentration, and to directly impact the supersaturation ratio of Zn(II) species. From these results, we identify the presence of three different growth regimes depending on the precursor concentrations, each of them giving rise to

ZnO nanowire arrays with specific morphological properties. These results highlight the critical importance of the thermodynamic properties of the chemical bath in the formation process of ZnO nanowires from Au seed layers, and provide key elements of understanding to efficiently optimize their morphology for their integration into piezoelectric devices.

1. INTRODUCTION

Devices based on the piezoelectric effect of nanostructures such as piezoelectric nanogenerators (PENGs) and sensors have received a large interest over the last 15 years.[1–5] In particular, zinc oxide (ZnO) nanostructures have gained a broad attention for their integration into such devices, as ZnO benefits from the advantages of being an abundant and biocompatible wide band-gap semiconductor (3.37 eV at room temperature) with relatively high piezoelectric constants (e_{33} = 1.34 C/m^2 and e_{31} = -0.57 C/m^2).[6] By using nanostructured ZnO in the form of vertically aligned, high aspect ratio nanowire (NW) arrays presenting sufficient surface densities, the piezoelectric effect is further significantly enhanced as compared to the use of bulk ZnO or thin films.[7] The resulting PENGs integrating such morphologically controlled ZnO NW arrays encapsulated in a polymer matrix between two metallic electrodes have the potential to autonomously supply low-power miniaturized portable devices in the range of the milliwatts.[3] Among the wide variety of physical and chemical deposition methods used for the synthesis of ZnO NWs,[8–14] chemical bath deposition (CBD) has gained much popularity as a low-temperature and low-cost scalable process compatible with any kind of rigid and flexible substrates.[15,16] CBD is a liquid phase growth method where the substrate is immersed in a sealed reactor containing an aqueous solution of appropriate chemical precursors, usually zinc nitrate ($Zn(NO_3)_2$) and hexamethylenetetramine (HMTA) in the case of ZnO synthesis, which is then heated at low temperature (< 100 °C) for several hours to activate the crystallization. To promote the heterogeneous nucleation of ZnO on the substrate and to ensure the formation of sufficiently dense arrays of ZnO NWs, a seed layer is typically pre-deposited on its surface. While polycrystalline thin films composed of ZnO nanoparticles are most commonly used as seed layers to obtain ZnO NW arrays with controlled morphologies,[17,18] metallic thin films acting as bottom electrodes such as polycrystalline Au are typically considered when integrating these NW arrays into piezoelectric devices due to the Schottky nature of the ZnO/Au interface, which is required to prevent current leakage through the device.[3,19–21] Despite the presence of several studies successfully integrating ZnO NW arrays grown from Au seed layers into PENGs,[20,22,23] their morphological control remains challenging and a deeper understanding of their formation mechanisms should thus be attained to obtain highly oriented ZnO NW arrays with optimal morphological properties for their efficient integration into piezoelectric devices.

In this context, our previous work thoroughly investigated the nucleation pathways of ZnO through the modification of the Au seed layer morphology.[21] We demonstrated that the nucleation of the *c*-axis oriented ZnO NWs is typically performed through their heteroepitaxy on top of the (111) Au free surfaces located on top of the

<111>-oriented grains to form a primary population of vertically aligned NWs. However, we also revealed the presence of a secondary population of ZnO NWs highly disoriented of around 20 ° with respect to the normal to the substrate surface – and thus detrimental for the performance of the piezoelectric device, which is presumably formed through the nucleation of ZnO on the (211) facets of Au grains.[21] To reach ZnO NW arrays with optimized morphological properties, various works have further studied the influence of different growth parameters on the morphological properties of ZnO NWs grown by CBD from Au seed layers, such as the chemical bath temperature,[22,24,25] the growth time,[22,24,25] the introduction of additives,[22,25–27] or the precursor concentrations.[24,25] For instance, Xu *et al.* observed a strong variation of the ZnO NW density with precursor concentrations, reaching a maximum of more than 1 NW/μm^2 for $Zn(NO_3)_2$ and HMTA concentrations of 5 mM.[24] Additionally, they noticed a significant increase of the surface area coverage of the ZnO NW array with precursor concentrations, suggesting a strong increase of the NW diameters. In another study, Xu *et al.* optimized the aspect ratio of the ZnO NWs through a statistical design of experiments where several growth parameters were varied simultaneously.[25] They showed that the aspect ratio can be greatly enhanced from around 10 – 14 with no particular optimization to 22.3 when the CBD is performed with 1 mM of precursor concentrations at 80 °C and during 30 h. Furthermore, it can be noted that the introduction of additives such as ammonia (NH_3) in the chemical bath can drastically affect the morphological properties, as revealed by Boubenia *et al.* where the introduction of NH_3 led to variations of ZnO NW densities within two orders of magnitude.[27] However, these systematic studies, while providing valuable information on optimal growth parameter values, have not identified the physico-chemical processes at work during the CBD of ZnO NWs that could explain the morphological variations observed.

In this work, we investigate the influence of the precursor concentrations, a key growth parameter in the formation of ZnO NWs grown by CBD from Au seed layers. $Zn(NO_3)_2$ and HMTA precursor concentrations are varied in equimolar proportions from 1 to 100 mM and the morphological properties of the obtained ZnO NW arrays are thoroughly analyzed from field-emission scanning electron microscopy (FESEM) images. To gain more insight into the physico-chemical processes at work during the CBD, *in situ* pH measurements are carried out and coupled with thermodynamic computations. From these data, the influence of each type of ion formed in the chemical bath is assessed on the pH value, and a new approach is developed to accurately determine the hydrolysis ratio of HMTA molecules in the whole range of precursor concentrations studied. From these results, a complete diagram of the formation mechanisms of ZnO NWs is established and related to the evolution of the thermodynamic properties of the chemical bath with the precursor concentration. These findings provide an in-depth understanding of the influence of the precursor concentration on the morphological properties of ZnO NWs grown by CBD. They further illustrate the dominant role of the hydrolysis process of HMTA molecules in the chemical bath on the formation mechanism of ZnO NWs, which should be considered for the fabrication of efficient piezoelectric devices.

2. EXPERIMENTAL SECTION

2.1. Deposition Techniques. The samples were fabricated following the same procedure as in our previous work,[21] which is represented in **Figure 1**. (100)-oriented silicon wafers were used as substrates, where the native oxide layer was removed through a 1 min-immersion in a buffered hydrofluoric acid solution (Honeywell) followed by a deionized water rinsing. Ti layers of 10 nm were first deposited by vacuum evaporation (Plassys MEB550, $P < 10^{-6}$ Torr) at a rate of 0.1 nm.s^{-1} to ensure the adhesion of Au on the silicon substrates. Au thin films of 50 nm were subsequently deposited at a rate of 0.25 nm.s^{-1}. The film thicknesses were monitored *in situ* using a quartz microbalance. Such Au thin films typically present highly <111>-textured polycrystalline microstructure with 48 nm average grain size and 0.6 nm RMS roughness (see Table 1 of Ref.[21]). NWs were synthesized by CBD on the as prepared substrates, where the Au thin films act as seed layers for the nucleation of ZnO. The samples were immersed face down in separate beakers sealed with glass pieces coated with Parafilm, and containing varying equimolar concentrations ranging from 1 to 100 mM of zinc nitrate hexahydrate ($Zn(NO_3)_2.6H_2O$, Sigma-Aldrich) and hexamethylenetetramine (HMTA, $C_6H_{12}N_4$, Sigma-Aldrich) in Milli-Q water (18.2 Ω·cm). The sealed reactors were then placed in a regular oven heated at 85 °C for 3 h. It can be noted that the CBD was performed without any stirring that could favor convection processes. At the end of the CBD, the samples were immediately removed from the solution, rinsed with Milli-Q water and dried with N_2.

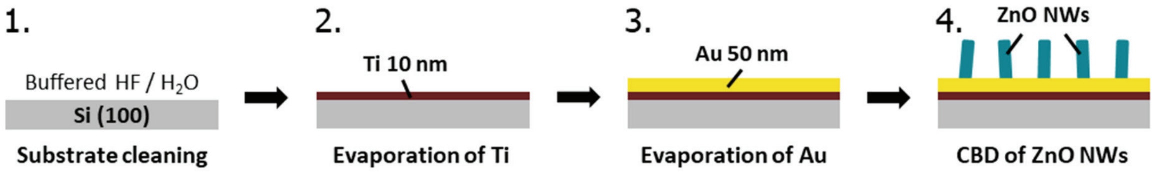

Figure 1. Schematic diagram representing the different steps required for the fabrication process of ZnO NWs on Au seed layers.

2.2. Characterization Techniques. The pH of the chemical bath was measured in an *in situ* manner throughout the CBD with an InLab Versatile Pro pH electrode from Mettler Toledo. The morphological properties of ZnO NWs were investigated with a FEI Quanta 250 field-emission scanning electron microscope (FESEM). For each sample, the mean lengths and diameters as well as the tilt angles of ZnO NWs were measured with the assistance of ImageJ software from cross-sectional view FESEM images on 100 NWs, while their mean surface densities were assessed from top-view FESEM images. The *c*-plane surface area ratios of ZnO NWs were also deduced from top-view FESEM images, and by further applying a filter generated by ImageJ software to only display their *c*-plane top facets.

2.3. Thermodynamic Computations. Thermodynamic simulations were performed using Visual MINTEQ software for determining the pH, the equilibrium concentration of NH_4^+ ions, as well as the supersaturation ratio of Zn(II) species in the chemical bath as a function of the precursor concentrations. Zn^{2+} ion was considered as a single metallic cation, which is able to form complexes with three possible ligands, namely NH_3, NO_3^-, and HO^-, denoted as L, by following the general reaction: $n\mathrm{Zn}^{2+} + i\mathrm{L} \leftrightarrow \mathrm{Zn}_n\mathrm{L}_i^{2n+}$ where $\mathrm{Zn}_n\mathrm{L}_i^{2n+}$ is the complex considered and i the coordination number. The global thermodynamic equilibrium was calculated from the stability constants $\beta_i^L = \frac{[Zn_nL_i^{2n+}]}{[Zn^{2+}]^n[L]^i}$ associated with each chemical reaction, whose the typical values at 25 °C were taken from NIST database and then deduced at 85 °C using the Van't Hoff equation. All the constants used in the computations are summarized in **Table S1**.

3. RESULTS AND DISCUSSION

3.1. Effects of the Precursor Concentration in the Chemical Bath on the Morphology of ZnO Nanowires. The structural morphology of ZnO NWs grown by CBD for 3 hours at 85 °C with equimolar concentrations of $Zn(NO_3)_2$ and HMTA ranging from 1 to 100 mM is presented in **Figure 2** by FESEM imaging, where strong morphological variations are revealed. To carefully quantify these variations, the mean length, diameter, and apparent density of a large number of ZnO NWs were systematically measured for each sample from such FESEM images, from which the NW aspect ratio, the total deposited volume, and the mean NW volume were deduced. The *c*-plane suface area ratio, defined as the ratio between the area of the *c*-plane top facets of ZnO NWs and the total area, was also assessed for each sample. The evolution of these morphological properties with the equimolar concentrations of $Zn(NO_3)_2$ and HMTA, denoted as C_0, is summarized in **Figure 3a**.

Interestingly, the precursor concentrations show a very limited influence on the mean length of ZnO NWs, as it remains included between 1.4 and 2.0 µm in the whole range of concentrations studied. The mean NW diameter slighlty decreases from 190 to 120 nm as C_0 increases from 1 to 50 mM, and then drastically increases up to 950 nm as C_0 reaches 100 mM. As a consequence, the NW aspect ratio remains roughly constant and is comprised between 9.9 and 13.4 as C_0 increases up to 50 mM, and then strongly decreases down to 2.0 as C_0 reaches 100 mM. The mean apparent density of ZnO NWs shows a rapid increase from 0.5 to 17.4 NW/µm^2 as C_0 increases from 1 to 50 mM, but then decreases down to 1.5 NW/µm^2 as C_0 reaches 100 mM. In contrast, the coverage ratio, defined as the *c*-plane top surface area ratio of the ZnO NW array, steadily increases from 0.02 to 0.54 as C_0 increases from 1 to 100 mM, which reflects the strong increase of the mean NW diameter despite lower NW surface densities occurring beyond 50 mM of precursor concentrations. The total deposited volume of ZnO exponentially increases from 0.023 to 1.7 µm^3/µm^2 as C_0 increases from 1 to 100 mM, which is consistent with the increasing amount of reactants available for the crystallization of ZnO. Furthermore, as the mean NW length is relatively constant, the evolution of the mean NW volume is directly correlated with the evolution of the mean NW diameter: this volume slightly decreases from 0.045 to 0.014 µm^3 as C_0 increases from 1 to 50 mM, and then drastically increases up to 1.1 µm^3 as C_0 reaches 100 mM.

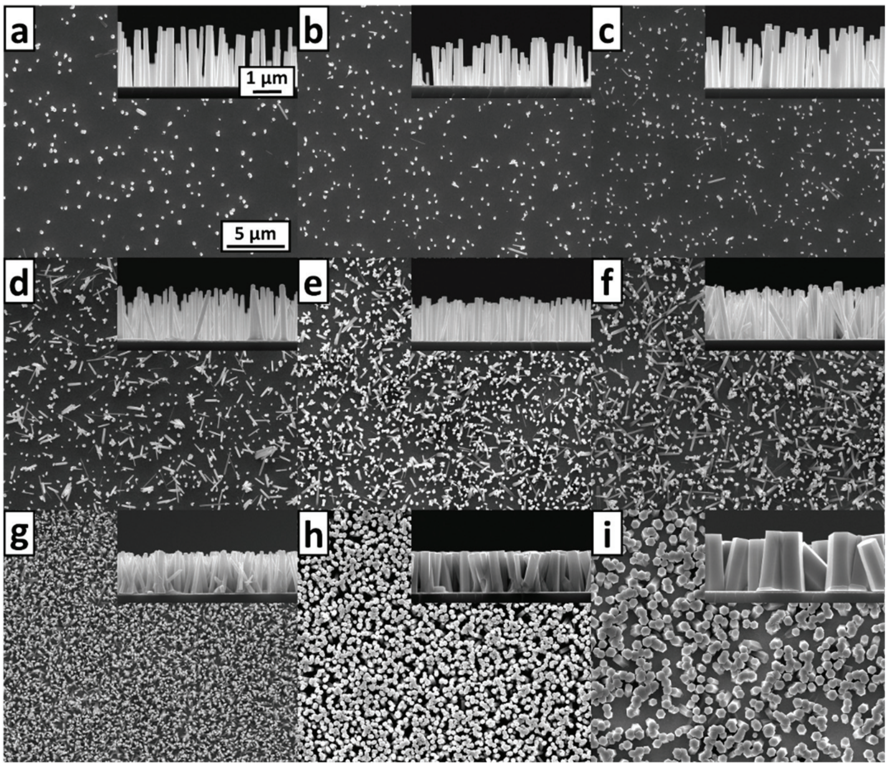

Figure 2. Top-view and cross-sectional view FESEM images of ZnO NWs grown by CBD for 3 hours at 85 °C with equimolar concentrations C_0 of $Zn(NO_3)_2$ and HMTA of (a) 1, (b) 3, (c) 5, (d) 10, (e) 20, (f) 30, (g) 50, (h) 80, and (i) 100 mM, respectively. Scales reported in (a) are valid for all top-view and cross-sectional view FESEM images, respectively.

The tilt angles of ZnO NWs with respect to the normal to the substrate were also systematically measured for each sample, from which their mean value and their distribution with respect to the precursor concentrations C_0 were deduced and reported in **Figure 3a** and **Figure 3b**, respectively. The mean tilt angle of ZnO NWs strongly increases from roughly 1 to 6 ° as C_0 increases from 1 to 10 mM, and then increases more progressively up to around 8 ° as C_0 reaches 100 mM. In our previous work, two distinct populations of ZnO NWs were identified when grown from Au seed layers : i) a primary population of well-oriented NWs with tilt angles typically below 5 ° nucleating from Au (111) facets, and ii) a secondary population of highly disoriented NWs with tilt angles typically comprised between 20 and 30 ° presumably nucleating from Au (211) facets.[21] To estimate the evolution of the verticality of the primary population of ZnO NWs, the mean tilt angles were also calculated for each sample by excluding any NW presenting a tilt angle greater than 15 °, as reported in **Figure 3a** (dashed line), thus removing any contribution from the highly disoriented secondary population. Up to precursor concentrations of 5 mM, we observe that the primary population of ZnO NWs has a mean tilt angle of around 1 ° and remains very close from the mean value calculated for all NWs, suggesting that the secondary population of NWs is negligible in this range of precursor concentrations. This is confirmed by the distributions of NW tilt angles for these precursor concentrations, as they reveal that more than 90 % of the NWs have tilt angles below 5 °. For precursor concentrations comprised between 5 and 50 mM, the mean tilt angle of the primary population of NWs increases progressively up to around 5 °. It can be noted that this value becomes greatly inferior to the value revealed for all NWs, which suggests that both primary and secondary populations of ZnO NWs coexist in this range of precursor concentrations. The NW tilt angle distributions show that, for precursor concentrations ranging from 10 to 30 mM, the proportion of NWs with high vertical alignment, *i.e.* with tilt angles below 5 °, is reduced to 70 – 80 %, while the presence of highly disoriented NWs with tilt angles comprised between 15 and 35 ° is clearly shown, confirming the appartition of the secondary population of NWs in this range of precursor concentrations. For precursor concentrations comprised between 50 and 100 mM, the mean tilt angle of the primary population of NWs remains roughly constant around 5 °. Additionaly, the proportion of NWs with high vertical alignment is further reduced, as only 45 to 50 % of the NWs have a tilt angle below 5 °. However, the remaining highly disoriented NWs show no preferential orientation for tilt angles in the range of 5 to 35 °. Thus, the primary and secondary populations of NWs are not clearly distinguishible in this range of precursor concentrations.

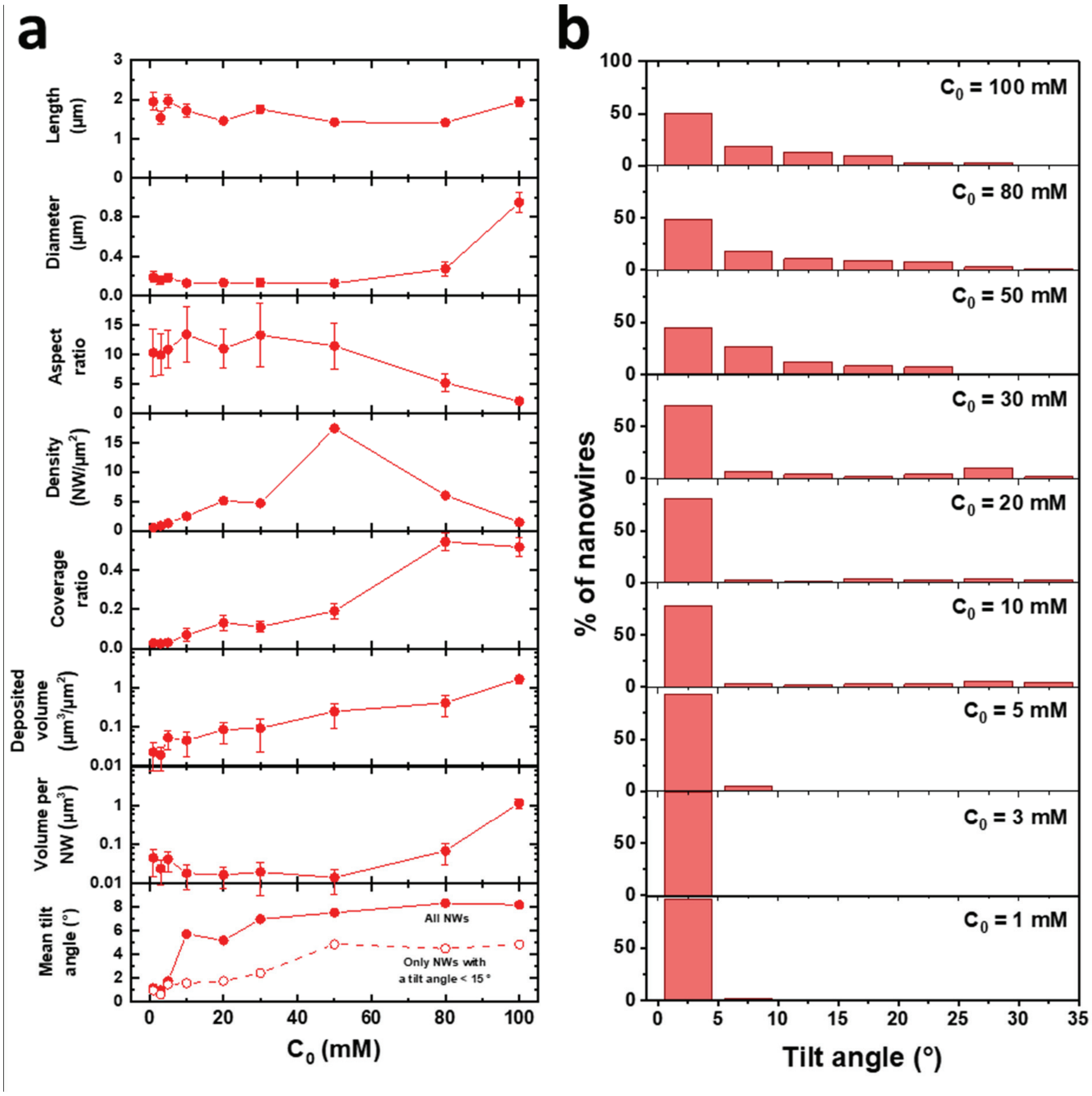

Figure 3. (a) Evolutions of the mean length, diameter, aspect ratio, apparent density, coverage ratio, total deposited volume, mean volume per NW and mean tilt angle of ZnO NWs as a function of the equimolar concentrations C_0 of $Zn(NO_3)_2$ and HMTA. (b) Histogram of the distribution of the NW tilt angles for each equimolar concentration C_0 of $Zn(NO_3)_2$ and HMTA studied.

3.2. Effects of the Precursor Concentrations in the Chemical Bath on its Thermodynamical Properties.

3.2.1. Evolution of the pH of the chemical bath. During the CBD of ZnO NWs, the thermodynamic properties of the chemical bath (*e.g.* distribution of aqueous species, or supersaturation ratio) play a crucial role on their nucleation and growth mechanisms. One of the key parameters influencing these thermodynamic properties is the pH of the chemical bath, as evidenced in Refs.[28–31] In this context, *in situ* pH measurements were performed during the CBD of ZnO NWs for C_0 values of $Zn(NO_3)_2$ and HMTA ranging from

1 to 100 mM, as revealed in **Figure 4a**. During the first 45 min of the growth, a strong decrease of the pH is observed regardless of C_0, and typically corresponds to the thermalization of the chemical bath up to the temperature setpoint of 85 °C. The pH of the chemical bath remains relatively stable for longer growth times with values ranging from 5.2 to 6.3 depending on C_0. A slight increase of the pH during the CBD process can however be observed for C_0 values ranging from 1 to 30 mM. This can be attributed to the progressive hydrolysis of HMTA molecules yielding the formation of additional HO^- ions according to the following chemical reactions:[16,32]

$$(CH_2)_6N_4 + 6H_2O \rightarrow 6HCHO + 4NH_3 \quad (1)$$

$$NH_3 + H_2O \leftrightarrow NH_4^+ + HO^- \quad (2)$$

This increase of pH value can also be associated with a slower kinetic of consumption of HO^- ions at the growing facets of ZnO NWs, which is directly related to the crystallization process as indicated by the following chemical reactions:[16,32]

$$Zn(NO_3)_2 \rightarrow Zn^{2+} + 2NO_3^- \quad (3)$$

$$Zn^{2+} + 2HO^- \leftrightarrow ZnO_s + H_2O \quad (4)$$

The rate of ZnO crystallization in the chemical bath is indeed known to decrease over time due to the progressive depletion of the reactants, as evidenced in Refs.[33,34].

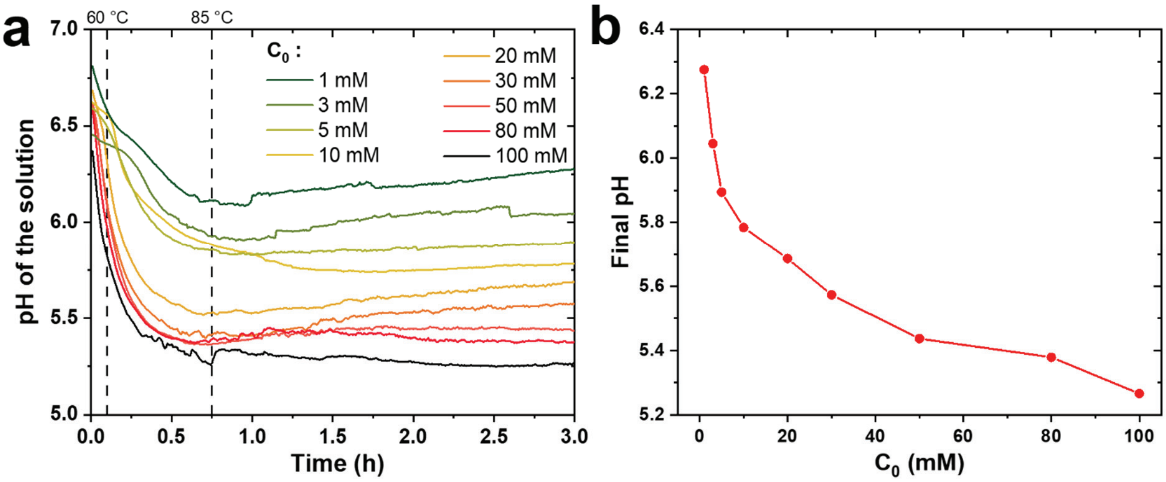

Figure 4. (a) Evolution of the pH during the CBD of ZnO NWs as a function of time for different equimolar concentrations C_0 of $Zn(NO_3)_2$ and HMTA in the range of 1 – 100 mM. (b) Final pH values measured at the end of the CBD as a function of C_0.

Interestingly, a significant reduction of the pH value occurs when C_0 is increased from 1 to 100 mM, as evidenced in **Figure 4b**. After 3 h of growth, the pH value ranges from 6.28 for C_0 = 1 mM down to 5.27 for C_0 =

100 mM. To understand this phenomenon, thermodynamic computations were performed with Visual MINTEQ software, from which the influence of each type of ions introduced in the chemical bath (*i.e.* Zn^{2+} and NO_3^- produced from the solubilization of $Zn(NO_3)_2$ in Eq.3 and NH_4^+ produced from the hydrolysis processes of HMTA and NH_3 molecules in Eq.1 and Eq.2) on the pH was identified. To do so, the pH at equilibrium was calculated for different sets of Zn^{2+}, NO_3^-, and NH_4^+ ion concentrations, as seen in **Figure 5**. Firstly, the concentrations of these ions were varied simultaneously in stoichiometric proportions to reproduce the case considered experimentally, where an equimolar concentration C_0 of chemical precursors is introduced in the chemical bath (black curve). While $Zn(NO_3)_2$ is usually completely solubilized through Eq.3 under standard CBD conditions (*i.e.* $[Zn^{2+}] = [NO_3^-] /2 = C_0$), the exact fraction of HMTA molecules undergoing the hydrolysis process through Eq.1 is not precisely known and is typically considered as ¼ to a first approximation. By further assuming the complete hydrolysis of NH_3 molecules through Eq.2, we thus consider that 1 mole of HMTA yields 1 mole of NH_4^+ ions (*i.e.* $[NH_4^+] = C_0$). From these assumptions, the obtained pH values are remarkably consistent with experimental data, as we observe a similar decrease of the pH when increasing the ion concentrations. The calculated pH at equilibrium varies from 5.50 at C_0 = 20 mM to 5.40 at C_0 = 40 mM, while the experimental pH of the solution measured after 1 h varies from 5.53 at C_0 = 20 mM to 5.40 at C_0 = 50 mM. Secondly, to thoroughly identify the role of each type of ions on the pH variations, several series of thermodynamic computations were performed, where the concentrations of either Zn^{2+} ions (red curve), NH_4^+ ions (green curve), or NO_3^- ions (blue curve) were swept independently. In each case, the concentrations of the two other types of ions were set to a reference concentration of 30 mM (for Zn^{2+} and NH_4^+ ions) or 60 mM (for NO_3^- ions). We can notice that the addition of Zn^{2+} ions has no influence on the pH value of the chemical bath at equilibrium since the solution is already saturated with Zn(II) species. The addition of NH_4^+ ions induces a slight increase of the pH value, which could be expected as NH_3 molecule is usually considered to experimentally increase the pH of the chemical bath from its hydrolysis process producing HO^- ions through Eq.2. However, the addition of NO_3^- ions leads to a significant decrease of the pH value, which counters the effect of NH_4^+ ions. Therefore, when increasing the precursor concentration C_0, the pH is subjected to the opposite effects of the increase of the NH_4^+ and NO_3^- ion concentrations. As a slight decrease of the pH value is overall observed, we can conclude that the influence of NO_3^- ions is dominant and explains the experimental variations of the pH observed as a function of C_0.

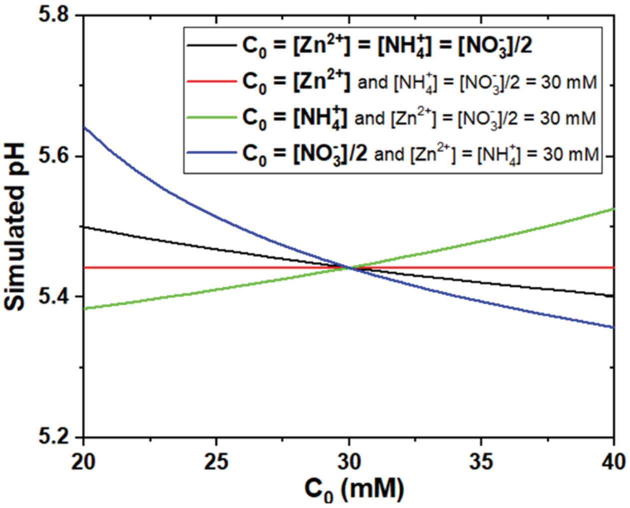

Figure 5. Evolution of the pH as a function of the concentrations of the different ions in the chemical bath, as computed by Visual MINTEQ software at 85 °C. For the black curve, the concentrations of every ion types (Zn^{2+}, NH_4^+, and NO_3^-) were varied simultaneously in stoichiometric proportions; for the red curve, only the concentration of Zn^{2+} ions was varied; for the green curve, only the concentration of NH_4^+ ions was varied; for the blue curve, only the concentration of NO_3^- ions was varied.

3.2.2. Determination of the HMTA hydrolysis ratio. HMTA molecule plays a central role in the CBD of ZnO NWs by acting both as a pH buffer of the solution through its progressive hydrolysis producing HO^- ions (*cf* Eqs.1 and 2)[35–37] and as a shaping agent favoring the growth along the polar *c*-axis through its presumable adsorption on the non-polar *m*-plane sidefacets.[32,38,39] The hydrolysis of 1 mole of HMTA is commonly assumed to yield 1 mole of NH_3, which is in turn hydrolyzed in 1 mole of NH_4^+ ions (*i.e.* the extents of reaction related to Eqs. 1 and 2 are of 0.25 and 1, respectively, as considered above in **Figure 5**) as it provides optimal supersaturation levels favoring the heterogeneous nucleation of ZnO NWs on the substrate.[28,32,33] However, the exact amounts of NH_3 and NH_4^+ ions produced in the chemical bath are typically not known despite their crucial importance to understand the evolution of the thermodynamic properties under different CBD conditions.

In this context, we propose here a method to accurately determine the actual concentration of NH_4^+ ions thanks to the pH values experimentally measured. To do so, additional thermodynamic computations were performed with Visual MINTEQ software, where the concentrations of Zn^{2+} and NO_3^- ions were varied in stoichiometric proportions (*i.e.* $C_0 = [Zn^{2+}] = [NO_3^-]/2$, with C_0 being the $Zn(NO_3)_2$ and HMTA concentrations in equimolar proportions), and where the concentration of NH_4^+ ions was adjusted so that the simulated pH values match the corresponding values experimentally measured for each precursor concentration C_0 between 1 and 3 h of growth time (*i.e.* when the chemical bath has fully been thermalized). The obtained values of the concentrations of NH_4^+

ions as a function of C_0 are presented in **Figure 6a**. We can notice that these values of the concentration of NH_4^+ ions are relatively close to C_0, which accounts for the previous assumption $[NH_4^+] = C_0$ as a first approximation. However, these values do not follow exactly this stoichiometry and are overall slightly greater than C_0. From these data, the actual hydrolysis ratio of HMTA molecules was further assessed and its evolution with C_0 is presented in **Figure 6b**. Interestingly, the hydrolysis ratio of HMTA molecules ranges from 20 % to values as high as 45 % when C_0 lies in the range of 1 – 100 mM. More specifically, it is maintained above 37 % for low values of C_0 below 10 mM, revealing that the hydrolysis ratio of HMTA molecules was significantly underestimated in this range of precursor concentrations. Moreover, the relative concentrations of NH_3 and NH_4^+ ions at each value of C_0 were extracted from the thermodynamic computations and reported as well in **Figure 6b** to estimate the hydrolysis ratio of NH_3 to NH_4^+ ions as described in Eq.2 and understand its impact on the overall reaction process. It appears that the hydrolysis ratio of NH_3 molecules is systematically above 97 % for any values of C_0 in the range of 1 – 100 mM, revealing that the vast majority of NH_3 molecules produced through Eq.1 is readily converted into NH_4^+ ions. The present approach comparing thermodynamic computations with experimental pH data thus appears as a powerful tool to thoroughly determine the chemical equilibrium and understand the behavior of complex systems.

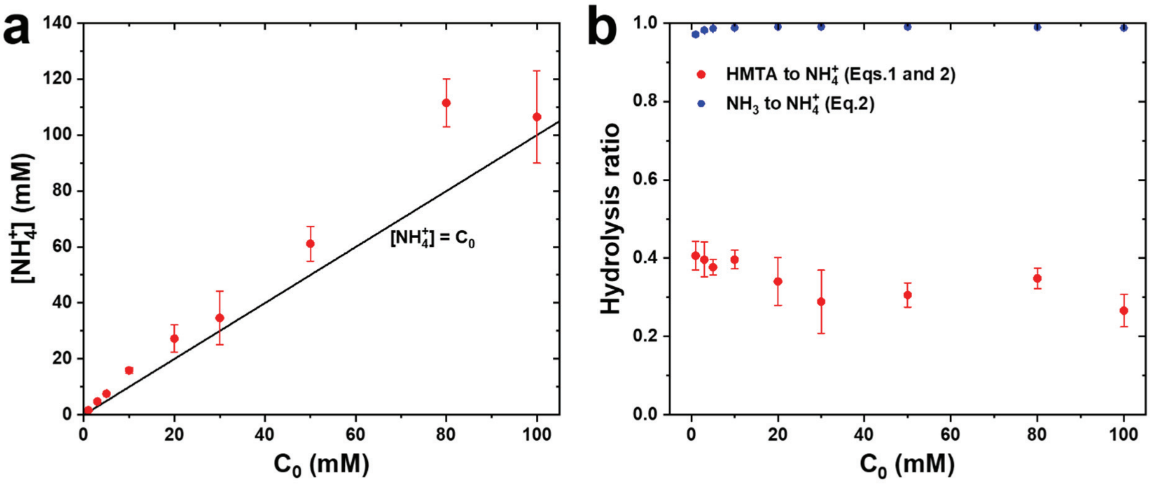

Figure 6. (a) Evolution of the concentration of NH_4^+ ions in the chemical bath as a function of the precursor concentrations C_0, for a temperature of 85 °C, as computed by Visual MINTEQ software by considering the *in situ* pH values measured between 1 and 3 h of growth time (see **Figure 4a**) as input data and assuming that C_0 is equal to the initial concentration of Zn^{2+} ions. The black line representing $[NH_4^+] = C_0$ is plotted as a visual help. (b) Evolution of the hydrolysis ratio of HMTA molecules to NH_4^+ ions through Eqs.1 and 2, and of NH_3 molecules to NH_4^+ ions through Eq.2 as a function of C_0.

3.2.3. Evolution of the supersaturation ratio. The supersaturation ratio, defined as $S_r = C_0/C_{eq}$, with C_0 and C_{eq} being the concentrations of Zn(II) species introduced in the chemical bath and at the thermodynamic equilibrium, respectively, is a key parameter for describing the nucleation and growth mechanisms of ZnO NWs. It is usually considered as the driving force for the crystallization process of ZnO.[40] When $S_r > 1$, the solution is supersaturated and the crystallization process of ZnO becomes thermodynamically favorable. However, C_{eq} is strongly dependent upon the composition of the chemical bath and the prior knowledge of the exact concentrations of the different chemical species is required for its calculation. For instance, it was shown that a small increase of the concentration of NH_4^+ ions leads to a drastic decrease of C_{eq}, and thus to a strong increase of the supersaturation ratio S_r.[28,29] This phenomenon is revealed as well in our thermodynamic computations, where S_r exponentially increases with the HMTA hydrolysis ratio at a given C_0 value, as shown in **Figure 7a**. Interestingly, it is also revealed that C_0 has a very limited influence on S_r in the range of 1 – 100 mM at a given HMTA hydrolysis ratio value. This shows that S_r is directly correlated with the evolution of the hydrolysis ratio of HMTA molecules, whereas it is almost not influenced by stoichiometric variations of Zn^{2+}, NH_4^+ and NO_3^- ion concentrations.

Thanks to the precise determination of the concentration of NH_4^+ ions produced from HMTA molecules performed for each value of C_0, it is possible to precisely quantify the experimental values of S_r in the chemical bath by extracting the value of C_{eq} from each corresponding thermodynamic computation. The variation of S_r as a function of C_0 is thus deduced and presented in **Figure 7b**. From these data, we observe a clear decrease of S_r from about 3.5 – 6.7 for $C_0 = 1$ mM to 1.8 – 2.5 for $C_0 = 100$ mM, which is consistent with the similar decrease of the hydrolysis ratio of HMTA molecules observed in **Figure 6b**. As a comparison, S_r values were also computed in the case of a constant hydrolysis ratio of HMTA molecules of ¼ (*i.e.* when $[HMTA] = [NH_4^+]$), where a constant value of nearly 2 was found for C_0 values ranging from 1 to 100 mM.

The supersaturation ratio is known to play a central role in the nucleation of solids in solution. In particular, when the solution is supersaturated ($S_r > 1$), the nucleation rate J of a given solid in solution is almost proportional to S_r according to the following equation:[40]

$$J = AS_r exp\left(-\frac{B}{ln^2 S_r}\right) \tag{5}$$

where A and B are two parameters dependent upon the temperature and the nature of the crystallizing solid. An increase of S_r induces in principle an increase of the density of nuclei. In the present case, the decrease of S_r observed when increasing C_0 from 1 to 100 mM seems to be in contradiction with the strong increase of the apparent density of ZnO NWs as observed in **Figure 3a**. However, in the context of the synthesis of ZnO NWs by CBD, two distinct types of nucleation should be considered: i) the homogeneous nucleation of NWs spontaneously crystallizing in the bulk of the chemical bath, and ii) the heterogeneous nucleation of NWs crystallizing from the seed layer of the immersed substrate.[41] It is thus important to note that, while the measured densities of ZnO NWs indicate an increase of the heterogeneous nucleation with C_0, the thermodynamic computations suggests that we simultaneously have a decrease of the overall nucleation rate (which includes homogeneous and heterogeneous nucleations). These trends can be explained by the lower formation energy typically required for a nucleus of ZnO during an heterogeneous nucleation process than during an homogeneous nucleation process.[40] When the supersaturation ratio becomes smaller (but still greater than 1), the heterogeneous nucleation, energetically more favorable, is favored at the expense of the homogeneous nucleation. Conversely, when the supersaturation ratio is higher, the rapid formation of numerous ZnO nuclei in the solution prevents the diffusion of the reactants towards the seed layer, which strongly favors the homogeneous nucleation.

As a consequence, the decrease of the supersaturation ratio observed when increasing the precursor concentrations leads to i) an overall reduction of the nucleation rate of ZnO NWs, and ii) an increase of the proportion of their heterogeneous growth from the Au seed layer at the expense of the homogeneous growth in the bulk of the solution. Interestingly, the nucleation of ZnO NWs by CBD from an Au seed layer is thus favored when the supersaturation ratio is small, which can be obtained by increasing the precursor concentrations. Nonetheless, it is worth noticing that the increase of the nucleation rate of ZnO NWs is not visible beyond precursor concentrations of 50 mM (see **Figure 2** and **Figure 3a**) due to the occurence of coalescence effects, reducing the apparent density of the NWs.

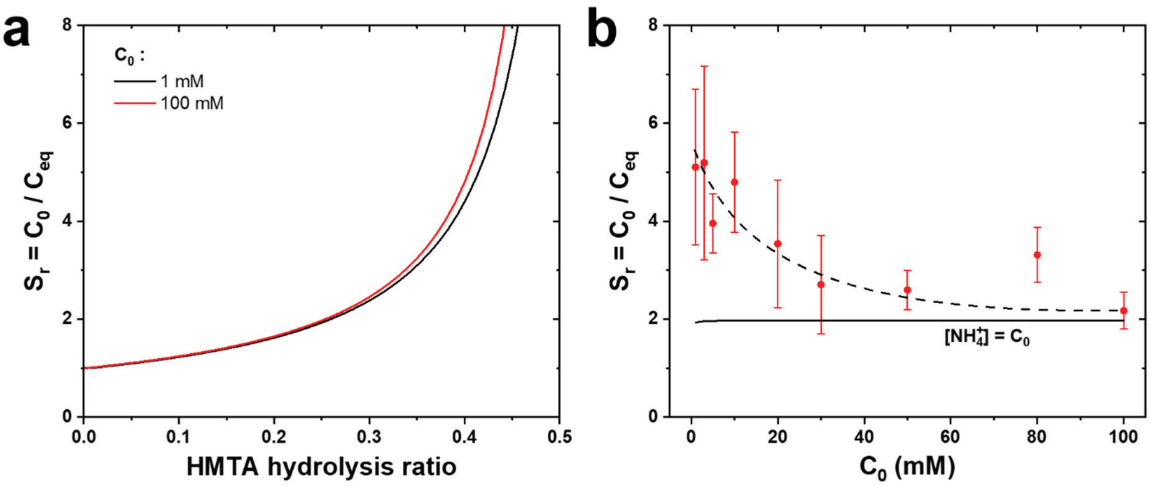

Figure 7. (a) Evolution of the supersaturation ratio S_r of Zn(II) species as a function of the hydrolysis ratio of HMTA molecules in the case where C_0 = 1 and 100 mM. (b) Evolution of S_r as a fonction of C_0 by considering for each value of C_0 the concentration of NH_4^+ ions obtained in **Figure 6a** (red dots). S_r values corresponding to the case where $[NH_4^+] = C_0$ are also indicated as a comparison (black line). The dashed curve serves as a visual help. The data were obtained from thermodynamic simulations at a temperature of 85 °C using Visual MINTEQ software.

3.3. Effects of the Precursor Concentration in the Chemical Bath on the Formation Mechanisms of ZnO Nanowires. In the light of these data, the formation mechanisms of ZnO NWs that most likely occur during each of the three growth regimes identified in **Section 3.1** are deduced and represented in **Figure 8**. When the precursor concentration C_0 is lower than 5 mM (**Figure 8a**), the hydrolysis ratio of HMTA molecules is high and leads to a high supersaturation ratio of Zn(II) species, which in turn leads to a low nucleation rate of ZnO NWs from the Au seed layer. The ZnO nuclei managing to form on the substrate are then sufficiently scarce to all occupy the most energetically favorable nucleation sites (*i.e.* those presenting the lowest nucleation barrier), which are the (111) free surfaces of the Au grains.[21] As the Au seed layer is also typically textured along the <111> direction,[21] the resulting ZnO NWs are hence very-well aligned vertically, which is characteristic of the primary population of NWs identified in Ref.[21]. When the precursor concentration C_0 lies in the range of 5-50 mM (**Figure 8b**), the hydrolysis ratio of HMTA molecules decreases, leading to a similar decrease of the supersaturation ratio of Zn(II) species, which in turn induces a higher nucleation rate of ZnO NWs from the Au seed layer. The number of ZnO nuclei is then much higher and cannot all occupy the most energetically favorable nucleation sites. For this reason, they presumably occupy nucleation sites on both the (111) free surfaces and (211) facets of Au grains, despite the fact that a higher nucleation barrier is associated with the latter one. These two types of nucleation processes lead to the formation of a majority primary population of ZnO NWs presenting high verticality and of a minority secondary population of ZnO NWs strongly disoriented of around 20 °, respectively, in a similar fashion as reported in Ref.[21]. When the precursor concentration C_0 is above 50 mM (**Figure 8c**), the hydrolysis ratio of HMTA molecules and the supersaturation ratio of Zn(II) species decrease slightly more, leading to an even greater nucleation rate of ZnO NWs from the Au seed layer. The ZnO nuclei thus presumably occupy, addionnally to the (111) free surfaces and (211) facets of Au grains, other nucleation sites exhibiting no preferential orientation. These nucleation sites could typically be other facets of Au grains or grain boundaries. Moreover, the density of ZnO nuclei being very high, ZnO NWs are subjected to coalescence effects from the very first stages of their growth, leading to the drop of their apparent density and to a strong increase of their diameter. As these NWs formed through various types of nucleation sites, they typically do not have any preferential orientation and thus no particular type of population can be distinguishible.

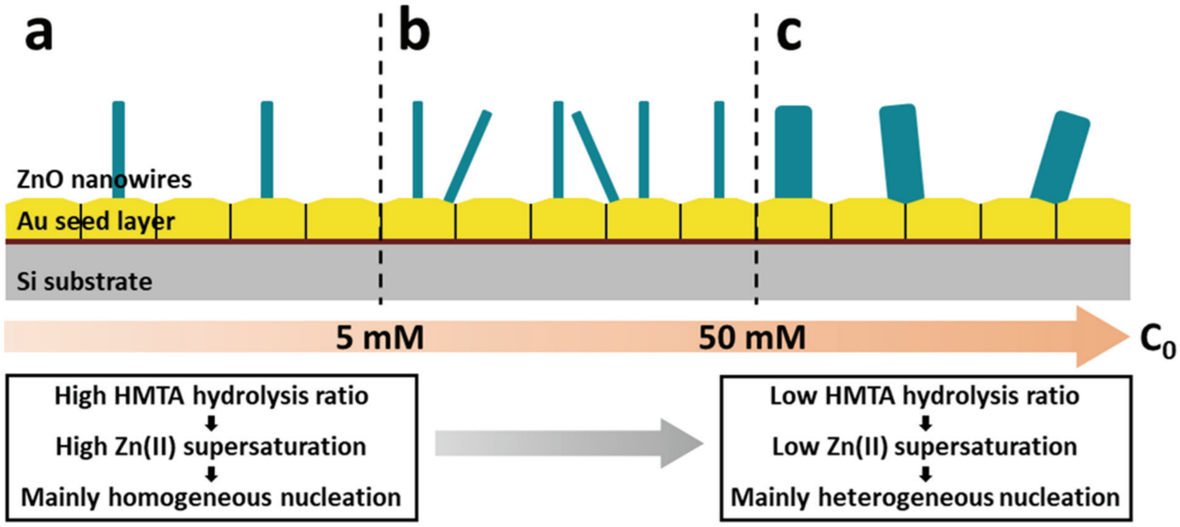

Figure 8. Schematic diagram of the formation mechanisms of ZnO NWs for different ranges of precursor concentrations C_0 : (a) $C_0 < 5$ mM, (b) 5 mM $\leq C_0 \leq$ 50 mM, and (c) $C_0 > 50$ mM.

4. CONCLUSIONS

In summary, the influence of the concentrations of the $Zn(NO_3)_2$ and HMTA precursors on the formation mechanisms of ZnO NWs grown by CBD from Au seed layers has thoroughly been investigated. Strong morphological variations of the ZnO NW arrays have been observed when varying the precursor concentration from 1 to 100 mM where a maximum apparent density of 17.4 NW/µm^2 was reached for 50 mM of precursors. By coupling *in situ* pH measurements of the chemical bath and thermodynamic computations, the evolution of the thermodynamic properties of the reaction medium with precursor concentration has carefully been analyzed to gain a fine understanding of the physicochemical processes at work during the formation of ZnO NWs. In particular, we have found that the decrease of the pH of the chemical bath with increasing precursor concentrations originates from the formation of NO_3^- ions through the decomposition of $Zn(NO_3)_2$. Moreover, the hydrolysis ratio of HMTA molecules has precisely been determined from these data, and found to decrease from approximately 37 – 45 % for low precursor concentrations below 10 mM to 20 – 30 % for higher precursor concentrations up to 100 mM. We have further revealed the major influence of the hydrolysis ratio of HMTA molecules on the supersaturation ratio of Zn(II) species in the chemical bath, which in turn strongly affects the crystallization process of ZnO. From these results, a complete growth diagram of the ZnO NWs has been established, where three different growth regimes are identified in the range of precursor concentrations studied. These findings reveal the crucial importance of the optimization of the thermodynamic properties of the chemical bath to obtain ZnO NW arrays of dedicated morphologies, and are highly valuable for their efficient integration into piezoelectric devices.

SUPPORTING INFORMATION

Data used for the thermodynamic computations.

AUTHOR INFORMATION

Corresponding authors

*E-mail: bassem.salem@cea.fr

*E-mail: vincent.consonni@grenoble-inp.fr

ORCID

Clément Lausecker: 0000-0001-8139-4029

Bassem Salem: 0000-0001-8038-3205

Xavier Baillin: 0000-0001-6750-5300

Vincent Consonni: 0000-0003-0171-8746

Notes

The authors declare no competing financial interests

ACKNOWLEDGEMENTS

This work was partially supported by the LabEx Minos under the contract ANR-10-LABX-55-01 and by the EquipEx IMPACT program, managed by the ANR French agency (ANR-10-EQPX-33). C.L. received a doctoral fellowship from the LabEx Minos. V.C. also acknowledges the financial support from the French National Research Agency through the projects ROLLER (ANR-17-CE09-0033) and DOSETTE (ANR-17-CE24-0003). This work has further benefited from some of the characterization equipment of the Grenoble INP–CMTC platform and has partially been supported by the French National Research Agency in the framework of the "Investissement d'avenir" program (ANR-15-IDEX-02) through the project CDP NEED. This work was also partly supported by the French RENATECH network.

REFERENCES

(1) Wang, Z. L.; Song, J. Piezoelectric Nanogenerators Based on Zinc Oxide Nanowire Arrays. *Science* **2006**, *312*, 242–246.

(2) Wang, X.; Song, J.; Liu, J.; Wang, Z. L. Direct-Current Nanogenerator Driven by Ultrasonic Waves. *Science* **2007**, *316*, 102–105.

(3) Wang, Z. L. Towards Self-Powered Nanosystems: From Nanogenerators to Nanopiezotronics. *Adv. Funct. Mater.* **2008**, *18*, 3553–3567.

(4) Briscoe, J.; Dunn, S. Piezoelectric Nanogenerators – a Review of Nanostructured Piezoelectric Energy Harvesters. *Nano Energy* **2015**, *14*, 15–29.

(5) Wang, Z.; Pan, X.; He, Y.; Hu, Y.; Gu, H.; Wang, Y. Piezoelectric Nanowires in Energy Harvesting Applications. *Adv. Mater. Sci. Eng.* **2015**, *2015*, 165631.

(6) Özgür, Ü.; Alivov, Ya. I.; Liu, C.; Teke, A.; Reshchikov, M. A.; Doğan, S.; Avrutin, V.; Cho, S.-J.; Morkoç, H. A Comprehensive Review of ZnO Materials and Devices. *J. Appl. Phys.* **2005**, *98* (4), 041301.

(7) Hinchet, R.; Lee, S.; Ardila, G.; Montes, L.; Mouis, M.; Wang, Z. L. Performance Optimization of Vertical Nanowire-Based Piezoelectric Nanogenerators. *Adv. Funct. Mater.* **2014**, *24*, 971–977.

(8) Sun, Y.; Fuge, G. M.; Ashfold, M. N. R. Growth of Aligned ZnO Nanorod Arrays by Catalyst-Free Pulsed Laser Deposition Methods. *Chem. Phys. Lett.* **2004**, *396*, 21–26.

(9) Huang, M. H.; Wu, Y.; Feick, H.; Tran, N.; Weber, E.; Yang, P. Catalytic Growth of Zinc Oxide Nanowires by Vapor Transport. *Adv. Mater.* **2001**, *13*, 113–116.

(10) Pan, Z. W.; Dai, Z. R.; Wang, Z. L. Nanobelts of Semiconducting Oxides. *Science* **2001**, *291*, 1947–1949.

(11) Heo, Y. W.; Varadarajan, V.; Kaufman, M.; Kim, K.; Norton, D. P.; Ren, F.; Fleming, P. H. Site-Specific Growth of ZnO Nanorods Using Catalysis-Driven Molecular-Beam Epitaxy. *Appl. Phys. Lett.* **2002**, *81*, 3046–3048.

(12) Wu, J.-J.; Liu, S.-C. Low-Temperature Growth of Well-Aligned ZnO Nanorods by Chemical Vapor Deposition. *Adv. Mater.* **2002**, *14*, 215–218.

(13) Park, W. I.; Kim, D. H.; Jung, S.-W.; Yi, G.-C. Metalorganic Vapor-Phase Epitaxial Growth of Vertically Well-Aligned ZnO Nanorods. *Appl. Phys. Lett.* **2002**, *80*, 4232–4234.

(14) Zheng, M. J.; Zhang, L. D.; Li, G. H.; Shen, W. Z. Fabrication and Optical Properties of Large-Scale Uniform Zinc Oxide Nanowire Arrays by One-Step Electrochemical Deposition Technique. *Chem. Phys. Lett.* **2002**, *363*, 123–128.

(15) Vayssieres, L.; Keis, K.; Lindquist, S.-E.; Hagfeldt, A. Purpose-Built Anisotropic Metal Oxide Material: 3D Highly Oriented Microrod Array of ZnO. *J. Phys. Chem. B* **2001**, *105*, 3350–3352.

(16) Xu, S.; Wang, Z. L. One-Dimensional ZnO Nanostructures: Solution Growth and Functional Properties. *Nano Res.* **2011**, *4*, 1013–1098.

(17) Yamabi, S.; Imai, H. Growth Conditions for Wurtzite Zinc Oxide Films in Aqueous Solutions. *J. Mater. Chem.* **2002**, *12*, 3773–3778.

(18) Guillemin, S.; Consonni, V.; Appert, E.; Puyoo, E.; Rapenne, L.; Roussel, H. Critical Nucleation Effects on the Structural Relationship Between ZnO Seed Layer and Nanowires. *J. Phys. Chem. C* **2012**, *116*, 25106–25111.

(19) Liu, J.; Fei, P.; Song, J.; Wang, X.; Lao, C.; Tummala, R.; Wang, Z. L. Carrier Density and Schottky Barrier on the Performance of DC Nanogenerator. *Nano Lett.* **2008**, *8*, 328–332.

(20) Xu, S.; Qin, Y.; Xu, C.; Wei, Y.; Yang, R.; Wang, Z. L. Self-Powered Nanowire Devices. *Nat. Nanotechnol.* **2010**, *5*, 366–373.

(21) Lausecker, C.; Salem, B.; Baillin, X.; Roussel, H.; Sarigiannidou, E.; Bassani, F.; Appert, E.; Labau, S.; Consonni, V. Formation Mechanisms of ZnO Nanowires on Polycrystalline Au Seed Layers for Piezoelectric Applications. *Nanotechnology* **2019**, *30*, 345601.

(22) Tian, J.-H.; Hu, J.; Li, S.-S.; Zhang, F.; Liu, J.; Shi, J.; Li, X.; Tian, Z.-Q.; Chen, Y. Improved Seedless Hydrothermal Synthesis of Dense and Ultralong ZnO Nanowires. *Nanotechnology* **2011**, *22*, 245601.

(23) Opoku, C.; Dahiya, A. S.; Oshman, C.; Cayrel, F.; Poulin-Vittrant, G.; Alquier, D.; Camara, N. Fabrication of ZnO Nanowire Based Piezoelectric Generators and Related Structures. *Phys. Procedia* **2015**, *70*, 858–862.

(24) Xu, S.; Lao, C.; Weintraub, B.; Wang, Z. L. Density-Controlled Growth of Aligned ZnO Nanowire Arrays by Seedless Chemical Approach on Smooth Surfaces. *J. Mater. Res.* **2008**, *23*, 2072–2077.

(25) Xu, S.; Adiga, N.; Ba, S.; Dasgupta, T.; Wu, C. F. J.; Wang, Z. L. Optimizing and Improving the Growth Quality of ZnO Nanowire Arrays Guided by Statistical Design of Experiments. *ACS Nano* **2009**, *3*, 1803–1812.

(26) Alenezi, M. R.; Henley, S. J.; Silva, S. R. P. On-Chip Fabrication of High Performance Nanostructured ZnO UV Detectors. *Sci. Rep.* **2015**, *5*, 8516.

(27) Boubenia, S.; Dahiya, A. S.; Poulin-Vittrant, G.; Morini, F.; Nadaud, K.; Alquier, D. A Facile Hydrothermal Approach for the Density Tunable Growth of ZnO Nanowires and Their Electrical Characterizations. *Sci. Rep.* **2017**, *7*, 15187.

(28) Verrier, C.; Appert, E.; Chaix-Pluchery, O.; Rapenne, L.; Rafhay, Q.; Kaminski-Cachopo, A.; Consonni, V. Effects of the PH on the Formation and Doping Mechanisms of ZnO Nanowires Using Aluminum Nitrate and Ammonia. *Inorg. Chem.* **2017**, *56*, 13111–13122.

(29) Gaffuri, P.; Appert, E.; Chaix-Pluchery, O.; Rapenne, L.; Salaün, M.; Consonni, V. The Path of Gallium from Chemical Bath into ZnO Nanowires: Mechanisms of Formation and Incorporation. *Inorg. Chem.* **2019**, *58*, 10269–10279.

(30) Lausecker, C.; Salem, B.; Baillin, X.; Chaix-Pluchery, O.; Roussel, H.; Labau, S.; Pelissier, B.; Appert, E.; Consonni, V. Chemical Bath Deposition of ZnO Nanowires Using Copper Nitrate as an Additive for Compensating Doping. *Inorg. Chem.* **2021**, *60*, 1612–1623.

(31) Villafuerte, J.; Sarigiannidou, E.; Donatini, F.; Kioseoglou, J.; Chaix-Pluchery, O.; Pernot, J.; Consonni, V. Modulating the Growth of Chemically Deposited ZnO Nanowires and the Formation of Nitrogen- and Hydrogen-Related Defects Using PH Adjustment. *Nanoscale Adv.* **2022**, *4*, 1793–1807.

(32) Parize, R.; Garnier, J.; Chaix-Pluchery, O.; Verrier, C.; Appert, E.; Consonni, V. Effects of Hexamethylenetetramine on the Nucleation and Radial Growth of ZnO Nanowires by Chemical Bath Deposition. *J. Phys. Chem. C* **2016**, *120*, 5242–5250.

(33) Lausecker, C.; Salem, B.; Baillin, X.; Consonni, V. Modeling the Elongation of Nanowires Grown by Chemical Bath Deposition Using a Predictive Approach. *J. Phys. Chem. C* **2019**, *123*, 29476–29483.

(34) Lausecker, C.; Salem, B.; Baillin, X.; Consonni, V. Implementing the Reactor Geometry in the Modeling of Chemical Bath Deposition of ZnO Nanowires. *Nanomaterials* **2022**, *12*, 1069.

(35) Govender, K.; Boyle, D. S.; Kenway, P. B.; O'Brien, P. Understanding the Factors That Govern the Deposition and Morphology of Thin Films of ZnO from Aqueous Solution. *J Mater Chem* **2004**, *14*, 2575–2591.

(36) Ashfold, M. N. R.; Doherty, R. P.; Ndifor-Angwafor, N. G.; Riley, D. J.; Sun, Y. The Kinetics of the Hydrothermal Growth of ZnO Nanostructures. *Thin Solid Films* **2007**, *515*, 8679–8683.

(37) McPeak, K. M.; Le, T. P.; Britton, N. G.; Nickolov, Z. S.; Elabd, Y. A.; Baxter, J. B. Chemical Bath Deposition of ZnO Nanowires at Near-Neutral PH Conditions without Hexamethylenetetramine (HMTA): Understanding the Role of HMTA in ZnO Nanowire Growth. *Langmuir* **2011**, *27*, 3672–3677.

(38) Sugunan, A.; Warad, H. C.; Boman, M.; Dutta, J. Zinc Oxide Nanowires in Chemical Bath on Seeded Substrates: Role of Hexamine. *J. Sol-Gel Sci. Technol.* **2006**, *39*, 49–56.

(39) Strano, V.; Urso, R. G.; Scuderi, M.; Iwu, K. O.; Simone, F.; Ciliberto, E.; Spinella, C.; Mirabella, S. Double Role of HMTA in ZnO Nanorods Grown by Chemical Bath Deposition. *J. Phys. Chem. C* **2014**, *118*, 28189–28195.

(40) Kashchiev, D.; van Rosmalen, G. M. Review: Nucleation in Solutions Revisited. *Cryst. Res. Technol.* **2003**, *38*, 555–574.

(41) Lincot, D. Solution Growth of Functional Zinc Oxide Films and Nanostructures. *MRS Bull.* **2010**, *35*, 778–789.

FOR TABLE OF CONTENT USE ONLY

Effects of Zinc Nitrate and HMTA on the Formation Mechanisms of ZnO Nanowires on Au Seed Layers

Clément Lausecker,[1,2,3] Bassem Salem,[2] Xavier Baillin,[3] and Vincent Consonni.[1*]*

[1] Université Grenoble Alpes, CNRS, Grenoble INP, LMGP, F-38000 Grenoble, France

[2] Université Grenoble Alpes, CNRS, CEA/LETI-Minatec, Grenoble INP, LTM, F-38054 Grenoble, France

[3] Université Grenoble Alpes, CEA, LETI, F-38000 Grenoble, France

Correspoding authors: bassem.salem@cea.fr and vincent.consonni@grenoble-inp.fr

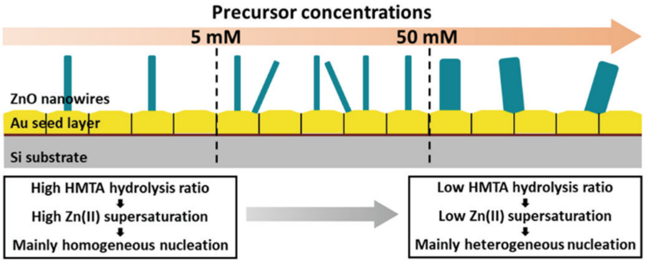

Synopsis

The formation mechanisms of ZnO nanowires grown by chemical bath deposition from Au seed layers were investigated for different $Zn(NO_3)_2$ and HMTA precursor concentrations. A new approach is further developed to determine the hydrolysis ratio of HMTA molecules by coupling *in situ* pH measurements and thermodynamic computations, revealing its drastic impact on the formation of ZnO nanowires.